PVK/MWNT Electrodeposited Conjugated Polymer Network Nanocomposite Films

Karina Milagros Cui,[†,‡] Maria Celeste Tria,[†] Roderick Pernites,[†] Christina A. Binag,[‡] and Rigoberto C. Advincula*[,†,‡]
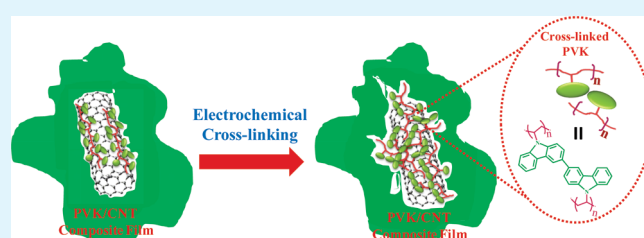
[†]Department of Chemistry and Department of Chemical and Biomolecular Engineering, University of Houston, Houston, Texas 772404-5003, United States

[‡]Graduate School, University of Santo Tomas, Manila, Philippines

Ⓢ Supporting Information

ABSTRACT: The facile preparation of poly (*N*-vinyl carbazole) (PVK) and multiwalled carbon nanotubes (MWNTs) solution and conjugated polymer network (CPN) nanocomposite film is described. The stable solutions of PVK/MWNT were prepared in mixed solvents by simple sonication method, which enabled successful deaggregation of the MWNTs with the polymer matrix. MWNT was most effectively dissolved in *N*-cyclohexyl-2-pyrrolidone (CHP) compared to other solvents like *N*-methyl pyrrolidone (NMP), dimethyl formamide, and dimethyl sulfoxide (DMSO). The composite solution was relatively stable for months with no observable precipitation of the MWNTs. Thermogravimmetric analysis (TGA) revealed the thermal stability of the nanocomposite while the differential scanning calorimetry (DSC) showed an increasing melting (T_m) and glass transition (T_g) temperatures as the fraction of the MWNTs in the nanocomposite was increased. Cyclic voltammetry (CV) allowed the electrodeposition of the nanocomposite film on indium tin oxide (ITO) substrates and subsequent cross-linking of the carbazole pendant group of the PVK to form CPN films. Ultraviolet−visible (UV−vis), fluorescence, and Fourier transform infrared (FTIR) confirmed film composition while atomic force microscopy (AFM) revealed its surface morphology. Four-point probe measurements revealed an increase in the electrical conductivity of the CPN nanocomposite film as the composition of the MWNTs was increased: 5.53×10^{-4} (3% MWNTs), 0.53 (5%), and 1.79 S cm^{-1} (7%). Finally, the interfacial charge transfer resistance and ion transport on the CPN nanocomposite film was analyzed by electrochemical impedance spectroscopy (EIS) with a measured real impedance value of ∼48.10 Ω for the 97% PVK and 3% MWNT ratio of the CPN nanocomposite film.

KEYWORDS: carbon nanotubes, nanocomposites, electrodeposition, thin film

■ INTRODUCTION

Polymer nanocomposites containing carbon nanotubes (CNTs) have received much interest due to its unique properties, such as high electrical conductivity, robust thermo-mechanical properties, and the potential to create new materials with improved characteristics coupled with a good chemical stability.[1−3] The CNTs used for these nanocomposites could either be single-walled nanotubes (SWNTs) or multiwalled nanotubes (MWNTs), the latter being more commercially relevant. However, effective utilization of the excellent properties of CNT-based composites depends on the quality of their dispersion and the level of polymer/CNT interfacial contact through covalent or noncovalent interactions. The use of π-conjugated polymers provides a tailored structure to interact with CNTs by means of π−π electronic interactions, which promotes better dispersion of CNTs.[4−7] Tang and co-workers also suggested that the enhanced solvating power of π-electron rich polymers for CNTs can be ascribed to the donor−acceptor mechanism, which results to the intimate contact of the polymer to the walls of the CNTs.[8,9] The additive effects of these interactions lead to the wrapping of the polymer backbone around the sidewalls of the CNTs that causes its dispersion.
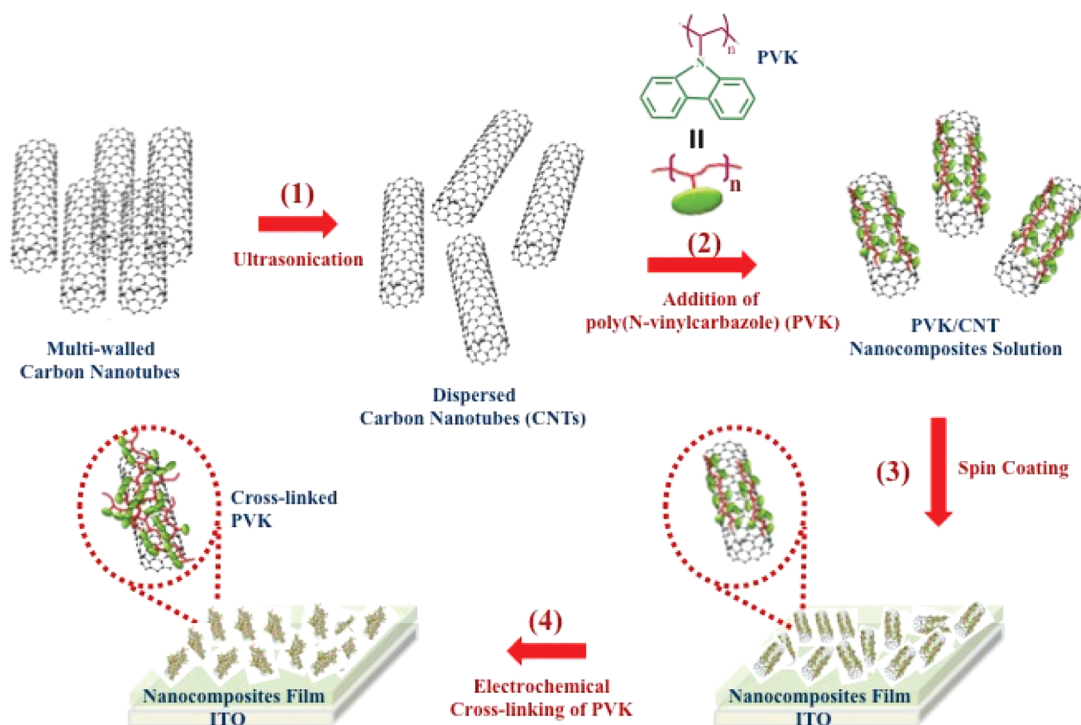
The formation of a homogeneous film of polymer/CNT nanocomposite has remained a great challenge because of the tendency of the CNTs to remain agglomerated. As the processing of CNT is generally hindered by their insolubility in most common organic solvents, only low weight/weight (w/w) or weight/volume (w/v) concentrations are usually obtained. For optimum transparent film preparation by casting, it is necessary to obtain a homogeneous dispersion of CNT in an organic solvent. One approach that has been commonly employed is the direct grafting of small molecules or polymers on the surface of the CNT, e.g. surface-initiated polymerization (SIP),[10] but with a resulting disruption of the primary structure of the nanotubes. Another procedure involves solution mixing of a dispersant polymer and CNT. This method is a convenient and facile route

Scheme 1. Schematic Representation Describing CNT Dispersion and CPN Nanocomposite Film Formation

and is highly desirable because the surface of the CNT is preserved during the process (i.e., the dispersant is only non-covalently adsorbed on the CNT).[5,10−12]

The combination of the unique properties of CNT and organic polymers like poly(*N*-vinyl carbazole) (PVK) makes it an interesting composite material for the development of practical semiconductor devices. PVK is well-known for its high chemical and thermal stability, photoconductivity, and opto-electronic properties, e.g., hole transporting properties.[13−16] It has been established that CNT could exhibit an amphoteric behavior by exchanging electrons with electron acceptors or electron donors to form the corresponding positive or negatively charged counterions.[17,18] Thus, the incorporation of CNT into the PVK matrix may be one of the interesting ways to extend the electro-optical properties of PVK and vice versa. Several studies have reported the preparation and characterization of different types of PVK/CNTs nanocomposites through chemical and electrochemical methods.[19−21]

The use of PVK to form the polymer/CNT nanocomposite could not only contribute to the unique properties of the composite but could also serve as a precursor polymer to electrodeposit a homogeneous film of nanocomposite on conducting surfaces. The Advincula group have reported a series of methods for depositing high optical quality ultrathin films of π-conjugated polymer network (CPN) system on a flat conducting substrate through the precursor polymer approach,[13−15,22] including electronanopatterning.[14] Combining this approach with the CNT nanocomposite film preparation would be of advantage because PVK can serve as both CNT dispersant and surface immobilizer at the same time.

In this work, we report the preparation of PVK/MWNT nanocomposites by sonication-dispersion of the MWNTs with PVK in a mixed solvent, spin-coating, and subsequent electrodeposition on surface by cyclic voltammetry (CV) (Scheme 1). The latter procedure leads to the formation of a CPN nanocomposite film. The method for accomplishing this result depends on an optimized dispersion of PVK and MWNT in a highly miscible solvent for both. This procedure involved a slow and continuous addition of dissolved PVK in a MWNT solution with the expectation that the PVK polymer chains wrap around the MWNT. These dispersions were then used to form spin-casted films that are electro-immobilized by CV to form cross-linked CPN nanocomposite films. The spectral properties of the PVK/MWNT nanocomposite were examined by UV−vis and fluorescence spectroscopy while thermal properties were analyzed using thermogravimetric analysis (TGA) and differential scanning calorimetry (DSC). The formation of the PVK/MWNT nanocomposite film was investigated by CV, UV−vis, electrochemical impedance spectroscopy (EIS), ATR spectroscopy, and atomic force microscopy (AFM). Four-point probe test was also used to probe conductivity behavior of the prepared films.

■ MATERIALS AND METHODS

A. Materials. The MWNTs (purity ≥95%) used in this study were obtained commercially from Baytubes (C150 P). The prepared MWNTs from Baytubes were produced in a high-yield catalytic process based on chemical vapor deposition (CVD). The outer and inner diameter, length, and density of the MWNTs were 13 nm, 4 nm, 1 μm, and 130−150 kg/m^3, respectively. The obtained MWNTs were further purified by heating at 200 °C for 6 h prior to use. Poly (*N*-vinyl carbazole) (PVK) was purchased from Sigma-Aldrich Chemicals (USA) (ca. MW = 50 000 g/mol). All solvents were of analytical grade and used without further purification and purchased from Sigma-Aldrich Chemicals or VWR: *N*-cyclohexyl-2-pyrrolidone (CHP), *N*-methyl pyrrolidone (NMP), dichloromethane (DCM), dimethyl formamide (DMF), and dimethyl sulfoxide (DMSO). Indium tin oxide (ITO)-coated glass plate (1 in. × 0.5 in.) was used as the substrate for PVK/MWNT nanocomposites and CPN film fabrication. The ITO-coated glass plates

were cleaned by sequentially sonicating the plates in deionized water, isopropanol, hexane, and toluene, each for 15 min, and the substrates were dried in an oven. The ITO-glass substrates were plasma cleaned for 3 min prior to their use.

B. Synthesis of PVK/MWNT Nanocomposites. The PVK/MWNTs nanocomposites were prepared using a solution mixing process. In a typical dissolution experiment, separate solutions of PVK in DCM and MWNTs in CHP with weight/volume (mg/mL) (w/v) concentration were first prepared. The purified MWNTs (5 mg/mL) was dissolved in CHP and ultrasonically agitated for 4 h. The PVK was dissolved in DCM using a sonication process for 30 min to disperse the PVK in the solvent. An appropriate amount of the PVK solution was slowly mixed to the MWNTs solution, which was followed by 1 h sonication. The PVK/MWNT dispersion was subjected to a high-speed centrifugation (4400 rpm, 1 h) and the black precipitate (mostly aggregates of MWNTs) obtained after centrifugation was removed. Methanol (5 mL) was then added to the remaining solution of the PVK/MWNTs dispersion. The mixture was then again placed in a high-speed centrifugation (4400 rpm, 30 min) and another batch of black precipitate was obtained. From the initial mass of PVK and MWNT used and the small amount of MWNTs that were removed after sonication/centrifugation, the final mass ratio of PVK to MWNT is 1:1. The above PVK/MWNTs precipitate was redispersed in CHP (mg/mL) followed by 20 min of ultrasonication, which produced a very stable PVK/MWNT solution.

C. PVK/MWNT Nanocomposite Film Fabrication. The PVK/MWNT nanocomposite solution was spin-coated on ITO substrate prior to its electrodeposition on the substrate. The spin-coating speed was decided depending on the viscosity of the prepared solutions. In a typical run, a thin PVK/MWNT film was spin-coated onto the ITO surface at a rate of 500 rms for 60 s and 1500 rms for 30 s consecutively to deposit a film on the ITO substrate surface. After spin-coating deposition, the PVK/MWNT nanocomposite films were thoroughly dried in vacuum oven for 24 h at 70 °C to remove any solvent.

After the deposition of the PVK/MWNT film through spin-coating, the film was electrochemically cross-linked using CV. CV experiments were carried out on a Princeton Applied Research Parstat 2263 using a three-electrode setup from a solution of 0.1 M LiClO$_4$ dissolved in acetonitrile (ACN). The coated ITO glass substrate was used as the working electrode (WE), Pt wire as the counter electrode (CE), and Ag/AgCl as the reference electrode (RE). Electrochemical cross-linking of PVK and MWNTs nanocomposite film was accomplished by repeatedly cycling the electrode potential between the potential range of 0 to 1.4 V for up to 50 cycles at a potential scan rate of 50 mV/s. The highly cross-linked nanocomposite film was thoroughly washed with ACN and was dried in nitrogen before its analysis.

D. Characterization of PVK/MWNT Nanocomposites and Films. All UV–vis spectra of the PVK/MWNT nanocomposite films and solutions were recorded using an Agilent 8453 spectrometer. Fluorescence spectra were obtained on a Perkin-Elmer LS-45 luminescence spectrometer. Thermal stability measurements of the prepared PVK/MWNT nanocomposites were performed using thermogravimetric analysis (TGA). The samples were heated from 20 to 900 °C at a heating rate of 20 °C/min on a TA Instruments 2950 thermogravimetric analyzer. All experiments were operated under a N$_2$ atmosphere at a purge rate of 80–90 mL/min. DSC measurements were carried out on all samples from 20 to 600 °C at a heating rate of 20 °C/min. TGA and DSC data were analyzed using TA Instruments' Universal Analysis software.

Attenuated total reflection (ATR) spectra were obtained using an FTS 7000 Digilab Spectrometer within the 700–4000 cm^{-1} range in multiple ATR geometry at the surface of the waveguide prism equipped with a liquid N$_2$-cooled MCT detector. The morphology before and after the electrodeposition of the PVK/MWNT nanocomposite on ITO substrates were characterized by atomic force microscopy (AFM). AFM imaging was done under ambient conditions with a PicoSPM II (PicoPlus,

Molecular Imaging - Agilent Technologies) using an intermittent contact mode. Scanning Electron Microscopy (SEM) was also used to determine the surface morphologies of the PVK/MWNT nanocomposite films. The micrograph images were observed by performing SEM investigation on a LEO 550 scanning electron microanalyzer. Silver sputtering of PVK/MWNT nanocomposite films were done using a silver coater to enhance the conductivity of the sample. Afterward, it was placed on copper stubs with carbon tape. The microscope chamber was maintained at a pressure below 1×10^{-6} Torr. The SEM filament was set at a voltage of 10 kV and a current of 5 nA using 200K× magnifications. The water contact angle of the films was measured using a KSV CAM 200 instrument utilizing a bubble drop method with water.

Electrochemical impedance spectroscopy (EIS) (Princeton Applied Research Parstat 2263) was used to investigate the ion-transport and dielectric/impedance properties of the PVK/MWNT nanocomposite and cross-linked PVK/MWNTs CPN films. EIS measurements were performed under an open circuit potential in an AC frequency range from 100 000 to 0.01 Hz with an excitation signal of 5 mV. All electrochemical experiments were carried out at room temperature. The DC conductivity of the PVK polymer alone and PVK/MWNT nanocomposite films were measured by an Alessi four-point probe method at room temperature (Keithley 2400). For the four-point probe test, a fixed current is injected into the substrate through the two outer probes and a voltage is measured between the two inner probes. The measured resistances were converted into conductivity first by multiplying the constant 4.532. The product is the sheet resistance in Ω/square of the film being measured. The calculated sheet resistance was multiplied by the film thickness to get the resistivity of the prepared film. Then the conductivity value was determined by taking the reciprocal of the resistivity. The data were represented by mean measurement values from at least 10 trials for every sample.

■ RESULTS AND DISCUSSION

Solution Characterization and Mixing Optimization. CNTs have unique structural, mechanical, thermal, and electronic properties, and have extensive applications in many fields.[1,23−25] However, the manipulation and processing of CNTs have been limited by their insolubility in most common organic solvents and their tendency to aggregate. UV–vis spectroscopy was first employed to gain insight on the developed solution-mixing and sonication method to disperse the MWNTs as visual-optical inspection of dispersions only indicates the presence or absence of particles that are larger than 10 μm. The UV–vis spectra were obtained under identical conditions and were diluted by the same factor so that qualitative comparisons between the different solvents could be made. The UV–vis absorbance of MWNT solutions using different solvents is presented in Figure 1a. All the solutions had the same starting concentration of MWNTs and the observed increase in absorbance indicates an increase in concentration of the unbundled MWNTs remaining in the solution after the sonication/centrifugation process. Different organic solvents (CHP, NMP, DMF and DMSO) demonstrated stable dispersions of MWNTs. From the UV–vis spectra (Figure 1a), however, it can be observed that CHP exhibited the highest absorbance as compared to NMP, DMF, and DMSO, signifying that CHP would be the most suitable solvent for the dispersion of MWNTs. The AFM image of the spin-casted solution of MWNT/CHP on mica depicts the deaggregation of the individual MWNT as shown in Figure 1b (see Figure S1 in the Supporting Information for comparison of MWNT in CHP before and after sonication).

The sonication process has been proven to be necessary in dispersing MWNTs in a solvent. However, excessive sonication
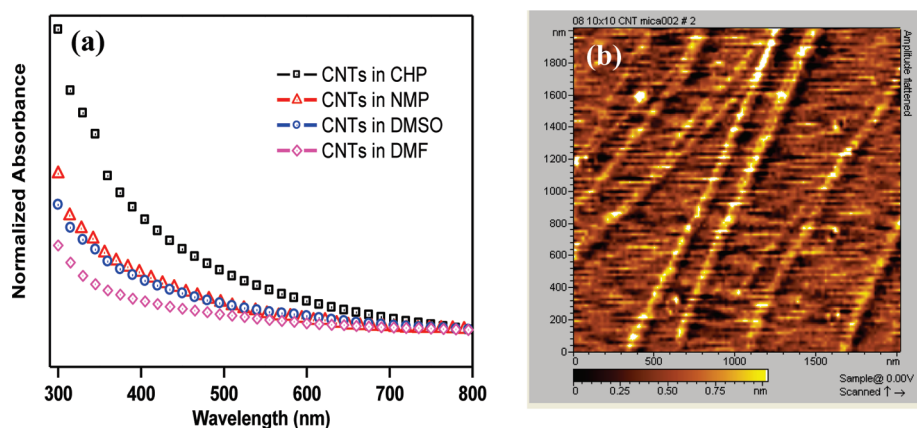
Figure 1. (a) UV—vis spectra of MWNT solution using different solvents at a concentration of 5 mg/mL. Spectra were taken after 24 h the solution had been sonicated for an hour. (b) The AFM image of a spin-cast dilute solution of CHP on mica.

has been reported to damage and cut the MWNTs.[26,27] To monitor the dispersion as a function of sonication time used in this work, UV—vis spectroscopy was also carried out as a function of time. With the increasing sonication time up to 4 h, the intensity of the whole spectral region increased and the dispersion of MWNTs became better (data not shown). Increasing the sonication time to 5 h, showed no significant difference in the absorbance as compared to 4 h sonication, which indicates that the concentration of the unbundled MWNTs in the solution approaches the solubility limit at this period. The SEM (see Figure S2 in the Supporting Information) and AFM analysis of the dispersed CNTs (Figure 1b) showed disentangled and long CNTs indicative that after sonication cutting was not observed in MWNTs (also see Figure S1 in the Supporting Information). Upon monitoring the absorbance of the sonicated MWNT in CHP for 4 h, it was observed that the dispersion was stable only up to 10 days (see Figure S3 in the Supporting Information), where the absorbance decreased after 11 days because of aggregation.

It has been identified that one of the most promising approaches to effectively disperse CNTs is through its functionalization with polymers that could prevent its agglomeration. However, this approach requires several tedious synthetic steps. The dispersion of MWNTs in PVK solution is an attempt to increase the solubility of MWNTs without going through the surface functionalization route but to induce adsorption through the wrapping of the PVK chains on the MWNTs. The polymer as a dispersant is usually more effective for MWNTs in organic solvents compared to small molecules or monomers. In this case, the carbazole units are expected to have better $\pi-\pi$ stacking properties on the benzenoid rings of the MWNTs surface and should have greater compatibility in terms of electro-optical properties. Thus, the dispersion containing well-dispersed and exfoliated MWNTs should lead to the preparation of PVK/MWNTs nanocomposites through a strong $\pi-\pi$ stacking interaction. One critical element is the formation of a homogeneous PVK/MWNT solution. The UV—vis of the PVK/MWNT nanocomposite in different organic solvents (CHP, DMSO, DMF, and NMP) are presented in Figure S4, showing distinct peaks between 320 and 350 nm assigned to the $\pi-\pi^*$ and n- π^* band of the carbazole moieties in PVK, which were not found in the MWNT solutions alone (Figure 1a). As described above, CHP is the most effective solvent for the MWNTs. CHP is also

miscible with DCM, which is a good solvent for PVK. By first preparing separate solutions of the MWNTs in CHP and PVK in DCM, relatively high concentrations of each component can be made. The solution composed of MWNTs, PVK, and the two miscible solvents was also aided by sonication, which plays a significant role in improving the interaction between the MWNTs and PVK. The homogeneity of the solution was proven by the clear and stable solution in mixed solvents (see Figure S5 in the Supporting Information). A possible explanation for the stable dispersion of MWNTs in the mixed solvent of CHP/DCM is that the PVK polymer chains are adsorbed to the MWNTs sidewalls due to strong $\pi-\pi$ electronic interactions between the aromatic pendants and the MWNTs surfaces.[4−7] Another reason is the donor—acceptor interaction between the PVK (donor) and the MWNTs (acceptor).[8,9] These interactions keep the MWNTs from its aggregation. Furthermore, the affinity of the polymer chains with the solvent leads to a more dispersed MWNTs in the organic solvents as presented in Figure S5 in the Supporting Information. The solution was stable for months without MWNTs precipitating out, which indicates effective solubilization of MWNTs by using PVK as the dispersant. The absorbance of PVK/MWNTs solution as a function of days was found to be stable even after 90 days of incubation of the prepared solution. The PVK/MWNTs nanocomposites also showed a good dispersion with other organic solvents (see Figure S6 in the Supporting Information).

The dispersion of PVK/MWNTs in mixed solvent system was affected not only by sonication time but also by the percentage weight of the final PVK/MWNTs solutions. The different percentages of MWNTs in PVK (3, 5, and 7%) were investigated in terms of dispersion and adherence on ITO glass substrate using the spin-coating technique as discussed in the next sections.

Analysis of the PVK/MWNT Nanocomposites in Solid-State or as Bulk Material. To confirm the formation (mixing) and the macromolecular interactions of the PVK/MWNTs solutions, TGA and DSC analyses of PVK/MWNTs of pure MWNTs, pure PVK, and different ratios of the PVK/MWNTs were conducted. The TGA thermograms of the pure MWNTs, pure PVK and different ratios of PVK/MWNTs nanocomposites were recorded under N_2 atmosphere scanned in the range of 20—900 °C (Figure 2). The TGA thermogram of pure PVK exhibited 2 degradation steps. The first degradation step takes place at 260 °C and then the polymer showed a fast second
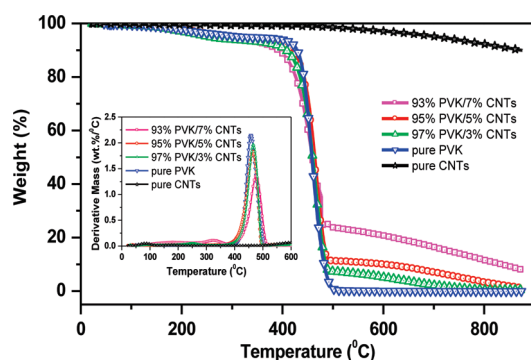
Figure 2. TGA thermograms of pure MWNTs, pure PVK, and PVK/MWNTs solutions under N_2 at a heating rate of 20 °C/min. (Inset) Graph of first derivative (dTGA) curves of pure MWNTs, pure PVK, and PVK/MWNTs nanocomposite solutions.

Figure 3. DSC curve of pure MWNTs, pure PVK, and PVK/MWNTs nanocomposites at a heating rate of 20 °C/min. (Inset) Graph showing the increase in T_m and T_g as the MWNTs loading increases.

degradation step reaching a 98% weight loss at 408 °C and almost total degradation at 455 °C. It is evident in the graph that the pure MWNTs exhibited a higher stability showing only a 2% weight loss even after heating the composite to 500 °C. For the 3 different compositions of PVK/MWNTs nanocomposites, the temperature of the distinct weight loss is lower compared to the pure PVK. The 7% MWNTs in PVK showed a lower % weight loss at 490 °C as compared to the two other ratios (5% and 3% MWNTs in PVK), which is attributed to the presence of more thermally stable MWNTs. It should be noted that the decrease in the % MWNTs leads to a more weight loss due to the higher composition of more degradable PVK at this temperature range. The first derivative TGA (dTGA) curves of various samples are also shown in Figure 2 (inset). The dTGA curves were added to identify the point where significant weight loss is most apparent. From the dTGA curves, it can be seen that there is a shift to higher degradation temperature for the PVK/MWNTs nanocomposites as compared to the pure PVK. Polymer chains near the nanotubes may degrade more slowly, which helps to shift the decomposition temperature to higher values.[19] Another possible reason is the increased thermal stability of the polymer composite due to the higher thermal conductivity of MWNTs that facilitates heat dissipation within the composite. An improvement in the thermal stability can be associated with a better dispersion of MWNTs, because it hinders the flux of decomposition product and thus delay the decomposition. It is important to point out that the difference in the extent of interaction between pure PVK and PVK/MWNT nanocomposites could be responsible for the higher thermal stability of the composites, i.e., the addition of MWNTs in PVK improves its thermal stability to degradation as compared to PVK alone.

To understand the difference in behavior of the nanocomposites as compared to pure PVK with respect to temperature, DSC analysis was also performed. Figure 3 shows the DSC traces of pure MWNTs, pure PVK and PVK/MWNTs nanocomposites. For pure PVK, the glass transition temperature (T_g) was observed at around 190 °C while the melting temperature (T_m) is found at 420 °C. The introduction of MWNTs into the PVK polymer matrix leads to an increase in the T_g and T_m, which could be due to high interfacial area of interaction between MWNTs and PVK that may lead to the decrease in the mobility of the outer polymer chain segments due to steric hindrance. This observation also presents further evidence of the wrapping around of the PVK chains to the MWNTs.
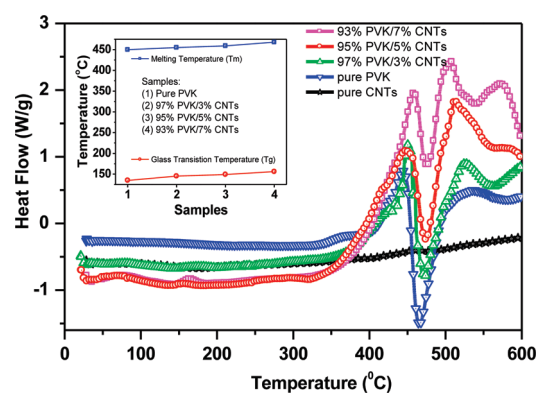
Electrochemical Deposition and Characterization of the PVK/MWNTs Nanocomposite Films and CPN Nanocomposite Films. CV electrodeposition, cross-linking, and characterization of the prepared PVK (control) and PVK/MWNTs nanocomposite films were done in 0.1 M $LiClO_4$ in ACN with potential scans between 0 and 1.2 V. The prepared solutions were spin-casted on the ITO-glass and Au substrate to directly measure the thickness of the film. Note that the spin-coated films are insoluble to ACN. The electrochemical cross-linking of the carbazole moieties was executed by employing CV. The reaction proceeded via a radical cation mechanism, typical of carbazolic moieties.[28,29] Figure 4 shows the cyclic voltammograms of pure PVK and PVK/MWNTs films scanned at different scan rates. For pure PVK (Figure 4a), an oxidation peak at about 0.9−1.0 V and a reduction peak at 0.7 V were observed in the voltammogram, which suggest the formation of the of carbazolylium radical cation, and a cross-linked material having more π-conjugated species compared to the PVK precursor. This result essentially represents the formation of a CPN control film. The scan rate dependence studies for PVK/MWNTs with different weight % at scan rates 50−200 mV/s is shown in Figure S7 in the Supporting Information. The current of the oxidation/reduction peaks were dependent on scan rates in the range of 50−200 mV/s. The electron transfer rate depends on the electron transfer resistance across the electrode/conductive polymer/electrolyte layer model. The shapes of the voltammogram were clearly different when the MWNTs were present together with the electrochemically cross-linked PVK. A downshift in the reduction peak was observed for PVK/MWNTs, which could be due to the doping behavior of the negatively charged MWNTs. No prominent anodic peak was observed regardless of the number of cycles employed during the deposition of the materials on the ITO substrate. The electrochemical cross-linking of PVK and MWNTs carried out at different scan rates shows a good correlation with the cathodic peak current and voltage scan rate indicating that the electron transfer is diffusion controlled. The electron transfer rate depends on the electron transfer resistance across the electrode/conductive polymer/electrolyte layer model. The PVK/MWNT CPN film exhibited a good linear relationship I and $v^{1/2}$. The slope of the plot is relative to the number of electrons in unit volume (n, cm^{-3}), diffusion coefficient (D, m^2/s), and the concentration of electrolyte ions (C_0, mol/cm^3), as indicated in the Cottrell equation

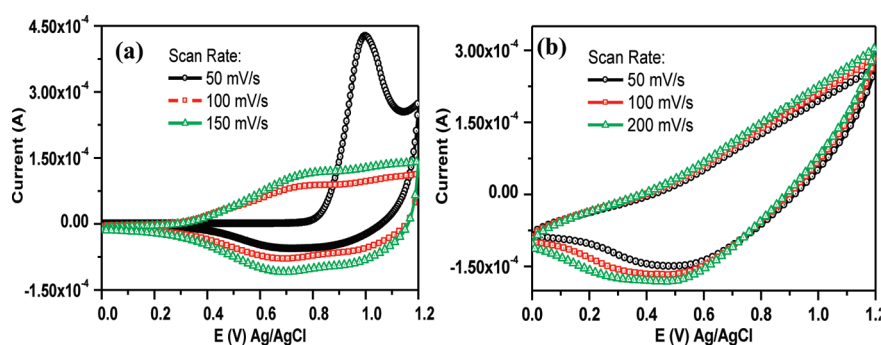$$I(t) = \text{NFAD}^{1/2} C_0 / \pi^{1/2} t^{1/2}$$

Figure 4. Cyclic voltammograms at different scan rates of (a) pure PVK and (b) 97% PVK/3% MWNTs (see Figure S7 in the Supporting Information for other compositions). In all cases, the first cyclic voltammogram is presented. Potentials reported against Ag/AgCl reference electrode.
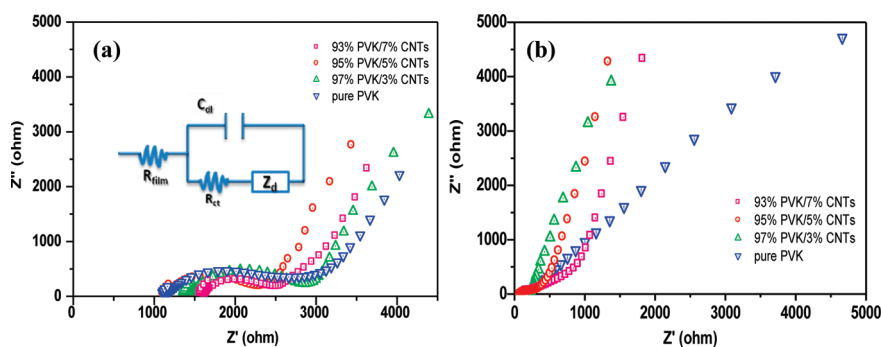

Figure 5. EIS nyquist plot of the PVK/MWNTs nanocomposite films prepared via spin-coating in ITO glass substrate: (a) PVK/MWNTs nanocomposites film and (b) PVK/MWNTs CPN nanocomposite films. The equivalent circuit is given in the inset graph.

The observed correlation is in agreement with the EIS analysis as will be discussed further. Figure S8 in the Supporting Information also shows that with increasing number of cycles, a gradual shift in peak potentials for the reduction peaks is indicative of the doping role of MWNTs, which would assume a negative charge.[21] Such a downshift in the cathodic peak could be due to the doping role of MWNTs, which are known to be amphoteric in character (can be doped with either electron donor or acceptor).[30] This observation in the CPN nanocomposite films, in which the PVK act as electron donor and MWNTs acts as the electron acceptor, needs to be taken into account.

Electrochemical Impedance Spectroscopy of the PVK/MWNTs and CPN Nanocomposite Films. EIS is a well-established and powerful tool for investigating interfacial charge-transfer in films. It is also useful for investigating ion-transport phenomena. The charge-transfer in nanocomposites can occur at both the interface between the PVK and MWNTs and the PVK and the electrodes used. To evaluate variations in interfacial properties of PVK/MWNTs, the qualitative differences in impedance spectra according to the different ratios of the MWNTs in PVK polymer matrix was considered. The equivalent circuit model for the working electrode employed and the physical significance of the components are presented in Figure 5 (inset graph). The equivalent circuit for this state is based on the modified Randles circuit, wherein the sum of the electrolyte resistance and polymer electronic resistance, C_{dl} electrolyte interface, R_{ct} the charge-transfer resistance and Z_d a complex circuit element is included. In this case, R_{film} is attributed primarily to the charge transfer resistance. As the percentage of the MWNTs in the composite increases, a 45° slope was observed which signals the presence of the Warburg element (Z_d),

representing the diffusion mass transport. At low frequencies, it is possible to estimate the faradaic pseudocapacitance (redox), which is associated with the capacitive behavior of a film. The physical origin of C_{dl} means that its magnitude increases with the quantity of the electroactive material deposited in the substrate. As presented in Figure 5a, in spite of the similar shape of the impedance spectra, an obvious difference in the diameters of the semicircles, which corresponds to the electron transfer-limited process measured at higher frequencies, the R_{ct} of PVK/MWNTs nanocomposites decreases as the loading of the MWNTs increased. The spectra prove that the formation of the charge-transfer complex of PVK/MWNTs nanocomposite occurs and that charge-transfer flows through the film. The complex plane impedance plots produced from the analysis of PVK/MWNTs CPN nanocomposite films are also presented in Figure 5b. The intercepts of the pure PVK and CPN nanocomposites film with the real impedance 55.78 Ω and for 97% PVK/3% MWNTs is 48.10 Ω. This result shows that the CPN nanocomposite film is 7.68 Ω less resistive than pure PVK. While this result is in agreement with a conductive contribution from the addition of MWNTs, this decrease in resistance could also be due to the formation of a π-conjugated CPN between the nanotubes and PVK polymer chains.

Spectroscopic Analysis. UV–visible spectra were used to characterize the interfacial interaction between the PVK/MWNT nanocomposite films and after the CPN nanocomposite film formation. As expected, no absorption peaks at the visible region of the electro-magnetic spectrum were observed for pure MWNTs, similar to the observation in solution. For the spin-casted nanocomposite film (Figure 6a), the main absorption bands occur at 331 and 345 nm, indicative of the π–π^* and
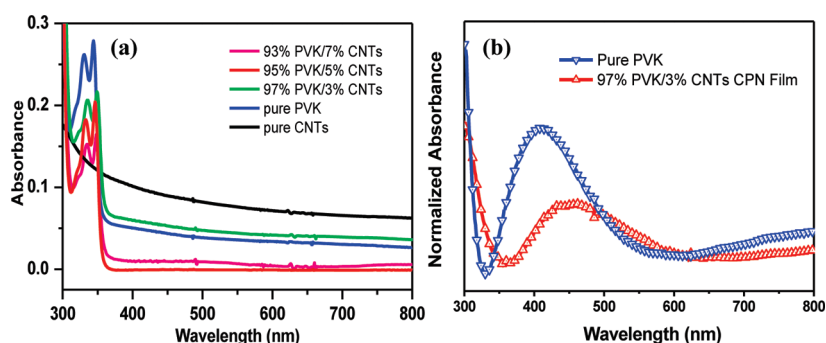
Figure 6. UV−vis spectra of (a) the spin-casted films of pure PVK and PVK/MWNTs nanocomposite and (b) the electrochemically cross-linked PVK and PVK/MWNTs CPN films.

n−π* attributed to optical transitions in pendant carbazole moieties of PVK. It can be seen from the spectra that the main absorption peaks for pure PVK is still prominent for the PVK/MWNTs nanocomposite. There is also a slight red shift of ∼5 nm in wavelength when MWNTs is incorporated in PVK (Figure 6a). This shifting may be attributed to the lowering of energy because of the electronic interaction between the PVK and MWNTs. The UV−vis absorbance after electrochemical cross-linking showed a different spectra due to the formation of π-conjugated oligocarbazole species (Figure 6b). The defined peaks for spin-coated PVK/MWNT film before cross-linking at 331 and 345 nm disappeared and a new band was formed at 440 and 760 nm, which corresponds to the polaronic and bipolaronic carbazole species.[28] The observation is consistent with previous works on electropolymerized PVK with the CPN approach.[13−15] The observed spectral red shift for the PVK/MWNTs CPN nanocomposite film after cross-linking can be attributed to the increase in π-conjugation and aided by the presence of MWNTs (serving as electron acceptor). Clearly further studies by spectro-electrochemistry will also be useful.

The fluorescence spectra of the films were also obtained using an excitation wavelength of 300 nm (see Figure S9 in the Supporting Information). From all the prepared films, the peak for PVK is clearly evident even in the nanocomposite films. It is known that PVK fluorescence spectra are broad and structure-less, which is the case observed from the spectra. The broad peak observed is a combination of the two emissions from the radio-active decay of two spectrally distinct excimers. The wavelength emission at 375 nm corresponds to the partially eclipsed config-uration of the PVK (i.e., only one carbazole moiety is aligned with the polymer backbone or between adjacent chains). On the other hand, the peak at 420 nm is attributed to the totally eclipsed conformation of the carbazole pendants (i.e., carbazole groups are aligned face-to-face in adjacent positions along the polymer backbone).[31,32]

ATR-IR Spectroscopy. IR spectroscopy is an important tool for confirming the presence of the components in the nanocom-posite film. The ATR spectra of pure MWNTs, pure PVK and 97% PVK/3% MWNTs CPN films spin-coated in ITO glass substrate are shown in Figure 7. The presence of interactions in the nanocomposite would shift the frequency of C−H stretching vibration of the polymer. For pure MWNTs, the peak at 1630 cm^{-1} is due to the C=C stretch mode in the MWNTs. The main absorption peaks of pure PVK structure are shown at the following characteristic bands at around 700−800 cm^{-1} (out-of-plane −C−H aromatic), 1100−1150 cm^{-1} (in-plane −C−H
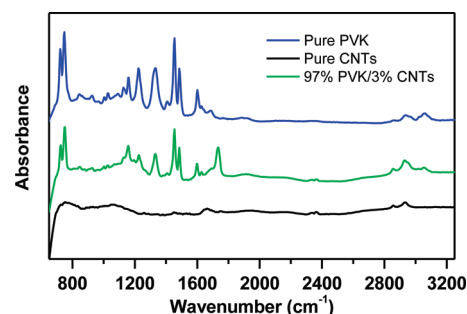

Figure 7. FT-IR-ATR spectra of PVK/MWNTs CPN films: (a) pure PVK, (b) 97% PVK/3% MWNTs CPN film, and (c) pure MWNTs.

aromatic), around 1600 cm^{-1} (C=C stretching), 2900 cm^{-1} (aliphatic C−H stretching), and 3050 cm^{-1} (aromatic C−H stretching). The peaks of pure PVK are attributed to the following vibrations: at 720 cm^{-1} (ring deformation of substituted aromatic structure), 744 cm^{-1} (>CH$_2$ rocking vibration due to tail-to-tail addition), 1159 cm^{-1} (out-of-plane deformation of vinylidene group and C−H in plane deformation of aromatic ring), 1220 cm^{-1} (C−N stretching of vinyl carbazole), 1326 cm^{-1} (>CH$_2$ deformation of vinylidene group), 1459 cm^{-1} (ring vibration of n-vinyl carbazole), and 1626 cm^{-1} (C=C stretching vibration of vinylidene group).

However, for the 97% PVK/3% MWNTs electropolymerized CPN film material, the peaks significantly changed at 744 and 1459 cm^{-1}. The addition of MWNTs in the PVK solution resulted to a new absorption band from 744 to 749 cm^{-1}, 1459 to 1449 cm^{-1}, and 1626 to 1620 cm^{-1}. The FTIR spectra of pure PVK and PVK/MWNTs CPN film show similar bands with a little variation in the stretching frequencies. The shift in the peak region between 700 and 1600 cm^{-1} is related to the change in the structure of the polymer upon the addition of the MWNTs.

Electrical Conductivity. One of the important methods to compare the state of nanotube dispersion at a given concentra-tion is through electrical conductivity measurements on films. The conductivity of pure PVK and PVK/MWNTs CPN nano-composite films at various compositions were measured using the four point probe conductivity test. For the four-point probe test, a fixed current is injected into the substrate through the two outer probes and a voltage is measured between the two inner probes. The measured resistances were converted into conduc-tivity by first multiplying the constant 4.532. The product is the

Table 1. DC Conductivity of Pure PVK and Various PVK/MWNT CPN Nanocomposite Film Compositions as Measured by the Four-Point Probe Technique

sample	measured conductivity (S/cm)[a]
(1) pure PVK	1×10^{-12}
(2) 97% PVK/3% MWNTs	5.53×10^{-4}
(3) 95% PVK/5% MWNTs	0.53
(4) 93% PVK/7% MWNTs	1.79
(5) 91% PVK/9% MWNTs	1.64

[a] Note: Mean conductivity at 10 measurements per sample.

Figure 8. AFM topography images and static water contact angles (inset) of the ITO-spin coated nanocomposite films of 97% PVK and 3% MWNTs (a) before and (b) after electrochemical cross-linking (50 cycles at 50 mV/s with scan range of 0−1.4 V).

sheet resistance in Ω/square of the film being measured. The calculated sheet resistance was multiplied by the film thickness to get the resistivity of the prepared film. The measured conductivity which is the reciprocal of resistivity is summarized in Table 1. A key issue in producing superior PVK/MWNTs nanocomposites is the ability to control deagglomeration and dispersion of MWNTs in PVK matrices, which are directly correlated with the achievable conductivity. The conductivity of PVK was about 1×10^{-12} to 1×10^{-16} S/cm, whereas with increasing MWNTs level, the conductivity increases. Dispersing the conducting filler, MWNTs in the polymer matrix forms a conductive polymer nanocomposite. The prepared CPN nanocomposite films of compositions 97% PVK/3% MWNTs, 95% PVK/5% MWNTs, and 93% PVK/7% MWNTs show conductivity values of 5.53×10^{-4}, 0.53, and 1.79 S/cm, which clearly shows a remarkable increase in conductivity. This increase in conductivity could be due to the formation of an interconnected network of MWNTs with the PVK matrix, which then permits a very high percentage of electrons to flow through a conductive path in the PVK/ MWNT composite film. However, by increasing the concentration of MWNTs in PVK solution to 9% by weight, the MWNTs started to agglomerate (data not shown). Insulating polymers are transformed to conductive composites by addition of MWNTs above a critical concentration or percolation threshold. When the positions of MWNTs in the polymer matrix form a conducting film, the conductivity of nanocomposites greatly increased, this may be due to the formation of a percolating network. Percolation means that at least one pathway of connected MWNTs exists in the sample which in case of conductive fillers allows the charge to flow through the sample. In conductive fillers like MWNTs, electrical measurements are suitable to detect the percolation composition. In this study, the percolation threshold was determined to be in the range of 3−5% MWNTs. In this range, the conductivity sigingficantly increases and the composites with MWNTs content higher than 5% weight can be regarded as electrically conductive. These values indicated that in the presence of 5% MWNTs in the PVK matrix is enough to form a network of conductive path. Above the percolation threshold concentration, 3% MWNTs independent fillers tend to link together to form conductive networks, which led to a significant increase in the conductivity of the prepared CPN nanocomposite films. The role of the CPN of the PVK is clear in comparison to the PVK alone.

The conductivity study of the nanocomposites shows that better dispersion of MWNTs in the polymer matrix greatly enhanced the conductivity. The absence of MWNTs sidewall damage and improved percolation in PVK/MWNTs CPN nanocomposite films led to an improvement in its electrical
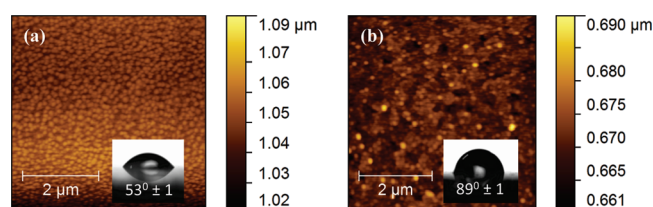
conductivity. Hence, this study suggests an effective way to improve dispersion of MWNTs into PVK matrices and also retain the electronic structure of MWNTs that could be used in various functional materials and coatings. In principle, utilizing single-walled nanotubes (SWNT) should even show a more remarkable change in conductivity and electro-optical properties assuming the same dispersion qualities.

AFM Imaging. AFM is a very useful tool for investigating the morphology of the modified surfaces because it provides information regarding spatial resolution, film topology, and nanostructure formation. The surface topography of PVK/MWNTs nanocomposites in terms of roughness values of the interfaces can also be analyzed by AFM. Figure 8, shows the topographies of PVK/MWNTs nanocomposite films deposited using spin-casting on ITO glass substrate before and after electrochemical crosslinking. The 97% PVK/3% MWNTs nanocomposite film (Figure 8a) showed elongated globular clusters that can be attributed to the presence of MWNTs (3% with respect to the composition of PVK) with an rms value of 3.11 nm. This result suggests a homogeneous wrapping of MWNT within the PVK polymer matrix is achieved, especially at the 97% PVK/3% MWNTs composition since no domains of MWNT were observed. The measured water contact angle was found to be $53.30° \pm 0.6$ in water. The PVK/MWNTs CPN nanocomposite film (Figure 8b) showed an rms value of 4.86 nm, which is also correlated to the decrease in the surface energy of the film as revealed in the measured WCA of $89.13° \pm 0.4$. The increase in the measured WCA indicates that a more hydrophobic PVK/ MWNTs CPN nanocomposite films was formed on the substrate after the electrochemical cross-linking.

■ CONCLUSIONS

PVK/MWNT nanocomposites were successfully prepared via solvent mixing process. The said process disrupted the van der Waals interactions between the bundled MWNTs upon the addition of the PVK dispersant, leading to a better dispersion of MWNTs in the PVK polymer matrix. The electrochemical cross-linking of the PVK/MWNTs nanocomposites may show the possible doping role and the charge-transfer interaction of the MWNTs in PVK/MWNT nanocomposite prepared via CPN film formation. The EIS spectra of the PVK/MWNTs nanocomposites fitted to a modified Randles circuit showed that the charge-transfer resistance decreases as the loading of MWNTs in PVK/MWNTs nanocomposites increases. ATR demonstrated the interaction between the PVK and MWNTs chains via the shifts observed in the vibronic spectra. The prepared nanocomposites also exhibited better thermal stability as revealed by the TGA and DSC data. The incorporation of a small weight percentage of MWNTs in the PVK polymer matrix relatively

increased the DC conductivity for all the composite systems. The electrical conductivity in the composites showed a 3% weight of MWNT minimum percolation threshold for the nanotubes, which indicates a good dispersion of MWNTs within PVK polymer matrix. The surface topography exhibited an improved uniformity for the nanocomposite films.

■ ASSOCIATED CONTENT

ⓢ Supporting Information.   AFM images of the spin-casted MWNTs before and after sonication, SEM image of the un-bundled MWNTs, UV−vis absorbance of the dispersed MWNTs in CHP for 11 days, UV−vis spectra of the PVK/ MWNTs nanocomposite solutions, digital images of the dispersed nanocomposites, CV of the other PVK/MWNTs ratio with respect to scan rate and number of cycles, fluorescence spectra of the PVK and PVK/MWNTs nanocomposites (PDF). This material is available free of charge via the Internet at http:// pubs.acs.org/.

■ AUTHOR INFORMATION

Corresponding Author
*E-mail: radvincula@uh.edu.

■ ACKNOWLEDGMENT

■ REFERENCES

(1) Sahoo, N. G.; Rana, S.; Cho, J. W.; Li, L.; Chan, S. H. *Prog. Polym. Sci.* **2010**, *35*, 837–867.

(2) Kanagaraj, S.; Varanda, F. R.; Zhil'tsova, T. V.; Oliveira, M. S. A.; Simoes, J. A. O. *Compos. Sci. Technol.* **2007**, *67*, 3071–3077.

(3) Grossiord, N.; Miltner, H. E.; Loos, J.; Meuldijk, J.; Van Mele, B.; Koning, C. E. *Chem. Mater.* **2007**, *19*, 3787–3792.

(4) Zhang, J.; Lee, J.-K.; Wu, Y.; Murray, R. W. *Nano Lett.* **2003**, *3*, 403–407.

(5) Baskaran, D.; Mays, J.; Bratcher, M. *Chem. Mater.* **2005**, *17*, 3389–3397.

(6) Yi, W.; Malkovskiy, A.; Chu, Q.; Sokolov, A.; Colon, M.; Meador, M.; Pang, Y. *J. Phys. Chem. B.* **2008**, *112*, 12263–12269.

(7) Reddy, K.; Sin, B.; Yoo, C.; Sohn, D.; Lee, Y. *J. Colloid Interface Sci.* **2009**, *340*, 160–165.

(8) Zhao, H.; Yuan, W. Z.; Tang, L.; Sun, J. Z.; Xu, H.; Qin, A.; Mao, Y.; Jin, J. K.; Tang, B. Z. *Macromolecules* **2008**, *41*, 8566–8574.

(9) Zhao, H.; Yuan, W. Z.; Mei, J.; Tang, L.; Liu, X. Q.; Yan, J. M.; Shen, X. Y.; Sun, J. Z.; Qin, A.; Tang, B. Z. *J. Polym. Sci., Part A: Polym. Chem.* **2009**, *47*, 4995–5005.

(10) Liu, P. *Eur. Polym. J.* **2005**, *41*, 2693–2703.

(11) Star, A.; Stoddart, J. F.; Steuerman, D.; Diehl, M.; Boukai, A.; Wong, E. W.; Yang, X.; Chung, s.-W.; Choi, H.; Health, J. R. *Angew. Chem., Int. Ed.* **2001**, *40*, 1721–1725.

(12) O'Connell, M. J.; Boul, P. J.; Ericson, L. M.; Huffman, C. B.; Wang, Y.; Haroz, E. H.; Kuper, C.; Tour, J. M.; Ausman, K. D.; Smalley, R. E. *Chem. Phys. Lett.* **2001**, *342*, 265–271.

(13) Baba, A.; Onishi, K.; Knoll, W.; Advincula, R. C. *J. Phys. Chem. B* **2004**, *108*, 18949–18955.

(14) Jegadesan, S.; Sindhu, S.; Advincula, R. C.; Valiyaveettil, S. *Langmuir* **2006**, *22*, 780–786.

(15) Fulghum, T. M.; Taranekar, P.; Advncula, R. C. *Macromolecules* **2008**, *41*, 5681–5687.

(16) Wang, S.; Yang, S.; Yang, C.; Li, Z.; Wang, J.; Ge, W. *J. Phys. Chem. B* **2000**, *104*, 11853–11858.

(17) Rao, A. M.; Eklund, P. C.; Bandow, S.; Thess, A.; Smalley, R. E. *Nature* **1997**, *388*, 257–259.

(18) Lee, R. S.; Kim, H. J.; Fischer, J. E.; Thess, A.; Smalley, R. E. *Nature* **1997**, *388*, 255–257.

(19) Maity, A.; Ray, S. S.; Pillai, S. K. *Macromol. Rapid Commun.* **2007**, *28*, 2224–2229.

(20) Liu, G.; Ling, Q.-D.; Teo, E. Y. H.; Zhu, C.-X.; Chan, D. S.-H.; Heoh, K.-G.; Kang, E.-T. *ACS Nano* **2009**, *3*, 1929–1937.

(21) Baibarac, M.; Lira-Cantu, M.; Oro Sol, J.; Baltog, I.; Casan-Pastor, N.; Gomez-Romero, P. *Compos. Sci. Technol.* **2007**, *67*, 2556–2563.

(22) Huang, C.; Jiang, G.; Advincula, R. C. *Macromolecules* **2008**, *41*, 4661–4670.

(23) Coleman, J. N.; Khan, U.; Gun'ko, Y. K. *Adv. Mater.* **2006**, *18*, 689–706.

(24) Wei, B. Q.; Vajtai, R.; Ajayan, P. M. *Appl. Phys. Lett.* **2001**, *79*, 1172–1174.

(25) Berber, S.; Kwon, Y.; Tomanek, D. *Phys. Rev. Lett.* **2000**, *84*, 4613–4616.

(26) Shin, H.-C.; Liu, M.; Sadanadan, B.; Rao, A. M. *J. Solid State Electrochem.* **2004**, *8*, 908–913.

(27) Lu, K. L.; Lago, R. M.; Chen, Y. K.; Green, M. L. H.; Harris, P. J. F.; Tsang, S. C. *Carbon* **1996**, *34*, 814–816.

(28) Ambrose, J. F.; Nelson, R. F. *J. Electrochem. Soc.* **1968**, *115*, 1159–1164.

(29) Macit, H.; Sen, S.; Sacak, M. *J. Appl. Polym. Sci.* **2005**, *96*, 894–898.

(30) Duclaux, L. *Carbon* **2002**, *40*, 1751–1764.

(31) Ye, T.; Chen, J.; Ma, D. *Phys. Chem. Chem. Phys.* **2010**, *12*, 15410–15413.

(32) Li., G. L.; Xu, L. Q.; Tang, X.; Neoh, K. G.; Kang, E. T. *Macromolecules* **2010**, *43*, 5797–5803.